JGR Space Physics

RESEARCH ARTICLE
10.1029/2020JA028587

Special Section:
Geospace multi-point observations in Van Allen Probes and Arase era

Global Magnetosphere Response to Solar Wind Dynamic Pressure Pulses During Northward IMF Using the Heliophysics System Observatory

S. E. Vidal-Luengo[1], and M. B. Moldwin[1]

[1]Department of Climate and Space Sciences and Engineering, University of Michigan, Ann Arbor, MI, USA

Key Points:

- Multisatellite observations of solar wind dynamic pressure pulses are tracked through the Earth's magnetosphere
- Propagating solar wind pressure pulse generates superposition of region specific signatures
- This paper provides the data base of all underlying data of all of the observations and analysis shown as a model for best data sharing

Correspondence to:
S. E. Vidal-Luengo,
svidal@umich.edu

Citation:
Vidal-Luengo, S. E., & Moldwin, M. B. (2021). Global magnetosphere response to solar wind dynamic pressure pulses during northward IMF using the heliophysics system observatory. *Journal of Geophysical Research: Space Physics*, *126*, e2020JA028587. https://doi.org/10.1029/2020JA028587

Received 15 AUG 2020
Accepted 29 DEC 2020

Abstract We analyzed the magnetospheric global response to dynamic pressure pulses (DPPs) using the Heliophysics System Observatory (HSO) and ground magnetometers. During northward Interplanetary Magnetic Field (IMF) Bz conditions, the magnetosphere acts as a closed "cavity" and reacts to solar wind DPPs more simply than during southward IMF. In this study we use solar wind data collected by ACE and WIND together with magnetic field observations of Geotail, Cluster, Time History of Events and Macroscale Interactions during Substorms (THEMIS), Magnetospheric Multiscale Mission (MMS), Van Allen Probes, GOES missions, and ground magnetometer arrays to observe the magnetosphere (dayside, nightside, inner magnetosphere, magnetotail, magnetosheath, etc.) and ionosphere response simultaneously in several local time sectors and regions. A total of 37 events were selected during the period between February 2007 to December 2017. We examine the global response of each event and identify systematic behavior of the magnetosphere due to DPPs' compression, such as MHD wave propagation, sudden impulses, and Ultra Low Frequency waves (ULF) in the Pc5 range. Our results confirm statistical studies with a more limited coverage that have been performed at different sectors and/or regions of the magnetosphere. We present observations of the different signatures generated in different regions that propagate through the magnetosphere. The signature of the tailward traveling DPP is observed to move at the same solar wind speed, and in superposition of other known magnetospheric perturbations. It is observed that the DPP also generates or increases the amplitude of Pc4-5 waves observed in the inner magnetosphere, while similar waves are observed on the ground.

Plain Language Summary The Earth's magnetosphere is similar to a balloon that is compressed by particles and magnetic field coming from the Sun. Similar to a drum, sudden increases in the amount and speed of particles coming from the Sun bangs the magnetosphere generating oscillations that propagate through the magnetosphere. In this study we use multiple satellite observations at different regions of the magnetosphere, and also ground-based observations to track and understand how different regions of the magnetosphere are affected by these sudden pressure changes. We find that, despite the big size of the magnetosphere, it is possible to track the compression throughout the system, and observe an increase in the amplitude of magnetic field oscillations.

1. Introduction

The solar wind is the main driver of Earth's magnetospheric structure and activity and determines the shape, location and dynamics of the magnetopause. Disturbances such as solar wind dynamic pressure pulses (DPPs), modify the size of the magnetosphere, while the Interplanetary Magnetic Field (IMF) strength and orientation determine how the solar wind disturbances affect the state of the magnetosphere (Nishida, 1983; D. G. Sibeck et al., 1991; Yu & Ridley, 2009). DPPs are characterized by an abrupt and large change of the solar wind density and/or velocity. These changes can be due to interplanetary discontinuities or shocks, Coronal Mass Ejections (CMEs), Corotating Interaction Regions (CIRs) or local perturbations in the solar wind. These disturbances generate a compression that is recorded by ground-based magnetometers as sudden impulses (SI), or storm sudden commencements (SSC) if they are followed by a geomagnetic storm. SIs and SSCs have been widely studied from multiple perspectives (Araki, 1977; Kokubun, 1983; Taylor, 1969; Huttunen et al., 2005). The magnetospheric response to DPPs under southward Bz IMF conditions differs from the response under northward Bz IMF (Dungey, 1961; Trattner et al., 2007). During southward Bz IMF, the DPPs compress the dayside magnetosphere in addition to enhancing low latitude magnetic

reconnection, increasing the influence of flux transfer events (FTEs) and substorms on the topology of the magnetosphere. FTE signatures at the magnetopause and ground are similar to the signatures generated by DPPs (D. D. Sibeck, 1990). However, during northward Bz IMF the magnetosphere reacts more simply to DPPs, majors storms are unlikely, and the magnetosphere is commonly compressed at all local time sectors (Zuo et al., 2015). The DPPs' compression generate fast-mode compressional waves that propagate through the magnetosphere faster than the magnetosheath flow, creating a bulge outward just before the compression associated with the DPP (D. Sibeck, 1990).

The response of the magnetosphere to DPPs has been studied in different local time sectors and regions. Borodkova et al. (2005) analyzed more than 300 events comparing solar wind observations by INTERBALL-1 and geosynchronous GOES satellites. They found that increases (decreases) in the dynamic pressure always result in increase/compression (decrease/decompression) in the geosynchronous magnetic field. Later, Borodkova et al. (2008) compared different events with three dimensional magnetohydrodynamic simulations, obtaining congruent results. Similarly, Lee and Lyons (2004) and Sanny et al. (2002) studied the geosynchronous magnetic response to DPPs during conditions of southward and northward Bz IMF. Lee and Lyons (2004) found that an increase in the dynamic pressure always leads to compression on the dayside. However, the nightside response shows a dependency on the IMF Bz direction. The nightside sometimes shows a dipolarization-like magnetic signature, but during northward IMF most of the cases show a compression. Sanny et al. (2002) found similar results, but also recognized that compression amplitudes are greater for northward IMF than for southward IMF.

The disturbances carried by the solar wind can also excite different types of ULF wave activity in the magnetosphere, such as Pc5 (periods between 150 and 600 s) and electromagnetic ion cyclotron (EMIC) waves (Claudepierre et al., 2010; Takahashi & Ukhorskiy, 2007; Usanova et al., 2012; Zhang et al., 2010). In other cases, the magnetosphere can act as a low-pass filter for the disturbances. Archer et al. (2013) show how sharp magnetosheath DPPs can induce compressional and toroidal modes and because each L-shell has their own oscillation mode in the Ultra Low Frequency (ULF) range, each L-shell partially filters high frequencies, in this way the whole magnetosphere acts as a low-pass filter. ULF waves play an important role for the magnetosphere-ionosphere coupling through particle-wave interactions (Elkington et al., 1999), and are also a mechanism to remotely study the magnetosphere (Ables & Fraser, 2005; Chi & Russell, 2005; Troitskaya & Bolshakova, 1988).

The study of the magnetotail is more complex due to the high apogee orbits of most of the missions available to perform in situ observations. In order to traverse the magnetotail, satellites need to be placed in very high and often very eccentric orbits, which allow them to perform only a few months of magnetotail observations each year. Despite this, there are several studies of the impact of DPPs in the tail. Petrinec and Russell (1993) developed an empirical model for the near-Earth magnetotail, using simultaneous observations of IMP-8 in the solar wind and magnetotail measurements performed by ISEE-1. Similarly, Collier et al. (1998) used IMP-8 and Yao et al. (2010) used one of the Double Star mission satellite, TC-1 to observe the tail response to DPPs during northward and weak southward IMF, showing a direct relationship between the solar wind dynamic pressure and tail magnetic compressions. Huttunen et al. (2005) used observations made by Cluster to study tail lobe SIs, finding that the disturbances were moving at speeds of order of the solar wind rather than Alfvén speed, which implies that the tail lobe SIs are generated by a compression of the magnetotail due to magnetosheath compression, instead of the transfer of magnetic flux from day-side through MHD waves. Similarly, Moldwin et al. (2001), used IMP 8 to show that DPPs can also generate a tailward moving South-then-North compression region signature, which are usually thought of as signatures of earthward propagating flux ropes (Moldwin & Hughes, 1994). The magnetospheric impact of DPPs can also be observed from ground magnetometer stations. Russell and Ginskey (1993, 1995) and Russell et al. (1994) showed the response to sudden impulses at different latitudes, while Slinker et al. (1999) and Kataoka et al. (2002) showed that magnetic signatures resulting from traveling convection vortices (TCVs) resulting from field-aligned currents (FACs) intensified by the magnetospheric compression due to DPPs. Similarly, Magnetic Impulse Events (MIEs) identified by Lanzerotti et al. (1991) as possibly intensification of FACs were studied with ground-based observations. Other studies showed the relationship between MIE occurrence and perturbations in the solar wind such as changes in the IMF and dynamic pressure (Konik et al., 1994; Lanzerotti et al., 1990).

Due to the lack of studies that observed multiple events that had simultaneous observations in different local time sectors and regions of the magnetosphere, previous studies were unable to observe the global magnetosphere response during DPPs. In this study we use eight different satellite missions and scores of ground-based magnetometers from middle to high latitudes in order to examine the global magnetosphere response to DPPs during northward IMF Bz conditions. Under these conditions, the magnetosphere acts as a closed "cavity" and reacts to solar wind dynamic pressure pulses more simply than during southward IMF conditions (Tsurutani & Gonzalez, 1995). The simultaneous observations of GOES, Geotail, Cluster, THEMIS, Van Allen Probes and Magnetospheric Multiscale Mission (MMS) missions as part of the Heliophysics System Observatory (HSO) makes possible the identification and tracking of propagating or traveling signatures, such as compression regions and waves, which can travel at different speeds and through different paths. Simultaneous ground magnetometer data are used to identify the ionospheric and field-aligned current response and signatures to DPPs.

The second section contains the methodology, where the criteria for the selection of events and identification of signatures are explained. It also describes the sources of data and the main characteristics of the missions used for this study. In the third section some statistical results are presented in order to set a context for the events shown in section four. The final sections contain the discussion of the results shown, including the analysis of the advantages and limitations of the HSO for the study of the magnetosphere. In the appendix we include a brief description of the data set and instructions to find the underlying and data created for this work, that was uploaded to the Deep Blue data service from the University of Michigan.

2. Data and Methodology

2.1. Data

The major part of the data consists of spacecraft and ground magnetic field vector measurements from February 2007 to December 2017. However, depending on the availability, plasma observations from spacecraft are also used to support the interpretation behind each signature observed. The data are obtained in Common Data Format (CDF; https://cdf.gsfc.nasa.gov/), Network Common Data Form (NetCDF; Rew and Davis (1990)) and ASCII files. All the satellite data except GOES mission data were obtained from the CDAWeb (http://www.cdaweb.sci.gsfc.nasa.gov). The CDAWeb also provides 1-min resolution OMNI data, which includes combined solar wind data parameters collected by ACE and WIND spacecraft. The SYM-H index is also obtained from OMNI. Most of the inner magnetosphere observations come from the GOES satellites. GOES magnetic data are found in the National Center for Environmental Information database (https://ngdc.noaa.gov/), whose files are in NetCDF format. The ground-based magnetometer observations come from a variety of observatories located above 60° magnetic latitude and accessed through SuperMag (http://supermag.jhuapl.edu/) available in ASCII format with a time resolution of 1-min. All the data used and created (including data found in every figure) for this study are included in a package of data uploaded to Deep Blue Data repository from the University of Michigan as an effort to improve reproducibility of our results.

2.1.1. Satellite Overview

The Heliospheric System Observatory satellite constellation consists of several missions. The Geostationary Operational Environmental Satellite (GOES). GOES-13 and GOES-15 provide observations of perturbation generated by the DPP in the inner magnetosphere (Singer et al., 1996). Van Allen Mission consist of two Radiation Belt Storm Probes (RBSP-A and RBSP-B) that study the Van Allen radiation belts with elliptic orbits with apogee around 6 Re (Spence et al., 2013). The Cluster II (hereafter just Cluster) mission consists of four spacecraft that as a result of their relative small spatial separation among them, are usually considered a single observation (however, we make use of the constellation to determine front orientations for several events when Cluster was in the solar wind). Cluster satellite have highly elliptical nearly polar orbits with an apogee around 20 Re. The Time History of Events and Macroscale Interactions during Substorms (THEMIS) is a five-satellite mission with highly elliptical orbits to study magnetic reconnection in the magnetotail. Two of the satellites broke the formation and were inserted into Lunar orbit (Angelopoulos, 2009) are now

called THEMIS-ARTEMIS. The MMS consists of four satellites orbiting Earth in a very close formation, we consider the constellation as a single observation except when used for multispacecraft timing of a perturbation. The mission also has a very elliptical orbit that allows observations around 12 Re in the dayside and 25 Re in the nightside. THEMIS and MMS orbits were used to explore day and night side simultaneously.

2.1.2. Ground Magnetometers Overview

The ground-based magnetometers correspond to multiple arrays of magnetometers around the world. The data are standardized by SuperMag to improve the access to the data. The data have 1-min resolution. For this study, we selected all station above 60° of magnetic latitude. The spatial density of the ground-based stations is larger in the Americas and Europe than in the rest of the world. This has the effect of limiting the local time coverage of ground-signatures.

2.2. Methodology

We developed and applied an algorithm to automatically detect potential DPP events. The algorithm searched for DPPs that occur during northward IMF and the set of conditions defined are focused on detection of clear, large amplitude events. False positive events are removed by visual inspection of the events. This is necessary as the time shifting done to ACE and WIND data in the OMNI database, and also data gaps can make it difficult to set conditions that apply correctly to all the data. The conditions are: (1) the increase of the SYM-H index must be larger than 6 nT; (2) the rise time must be in less than 3 min; (3) the SYM-H increase must occur during northward IMF that stay for at least 3 min (this identified 198 events); (4) DPPs occurrence confirmation in each event by visually inspecting the SYM-H index, solar wind dynamic pressure, interplanetary magnetic field, solar wind flow speed, and the magnetic field for each satellite. During this final inspection, events with $\frac{\Delta P}{P} > 1$ (reducing the number of events to 104) and five or more satellites in the magnetosphere (previous to the DPP) that observe a clear signal that can be associated to the DPP (usually but not necessarily, due to previous calm conditions) were selected for final analysis. This signal could be an increase in the total magnetic field, sudden magnetic field rotation, or increase in wave the activity. The $\frac{\Delta P}{P}$ ratio is computed by dividing the difference between the maximum dynamic pressure after the DPP and the dynamic pressure immediately before the DPP, by the dynamic pressure immediately before the DPP. The main reason we use SYM-H index as indicator of possible DPP occurrence is because this index is obtained from ground-based magnetometers, which allow us to narrow down to a minute the interval where the DPP hits the magnetosphere, for any of the propagation modes proposed in literature (Chi et al., 2001). Using these conditions, a total of 37 events were identified, this event collection allows the identification of global magnetospheric patterns due to dynamic pressure pulse propagation that could not be identified by using single observations and enables examination of conclusions made by statistical studies with simultaneous observations throughout magnetosphere. The conditions set favored the detection of events with large DPP during quiet conditions. Figure 1 shows the location of all satellites for the 37 events, using Shue et al. (1998) as reference for the magnetopause under nominal solar wind conditions. The list of the events is shown in Table 1. The locations of the satellite are mainly in the inner magnetosphere, but several spacecraft are in the solar wind, magnetosheath and the tail lobes, including THEMIS-B, C that made measurements of the far tail.

We examined the impact of the selection criteria with respect to the angle between the Earth's magnetic dipole axis and IMF of the selected events. We built histograms for the angle between IMF projected to the ZY (GSE) plane and the dipole axis. No major differences are found in the distribution of the angle between selected and nonselected events. This is probably due that our main selection criteria are events where the dynamic pressure change is large ($dP/P > 1$). As the effect of the dynamic pressure is likely larger than the angle between the dipole and the IMF, the potential influence of this angle was not captured.

The observations collected by satellites and ground-based magnetometer were classified by local time: dayside (9-15 LT), dusk (15-21 LT), midnight (21-3 LT), dawn (3-9 LT). Additionally, the satellites were also classified by radial distance and region (inner magnetosphere, magnetosheath, solar wind, tail lobe). We

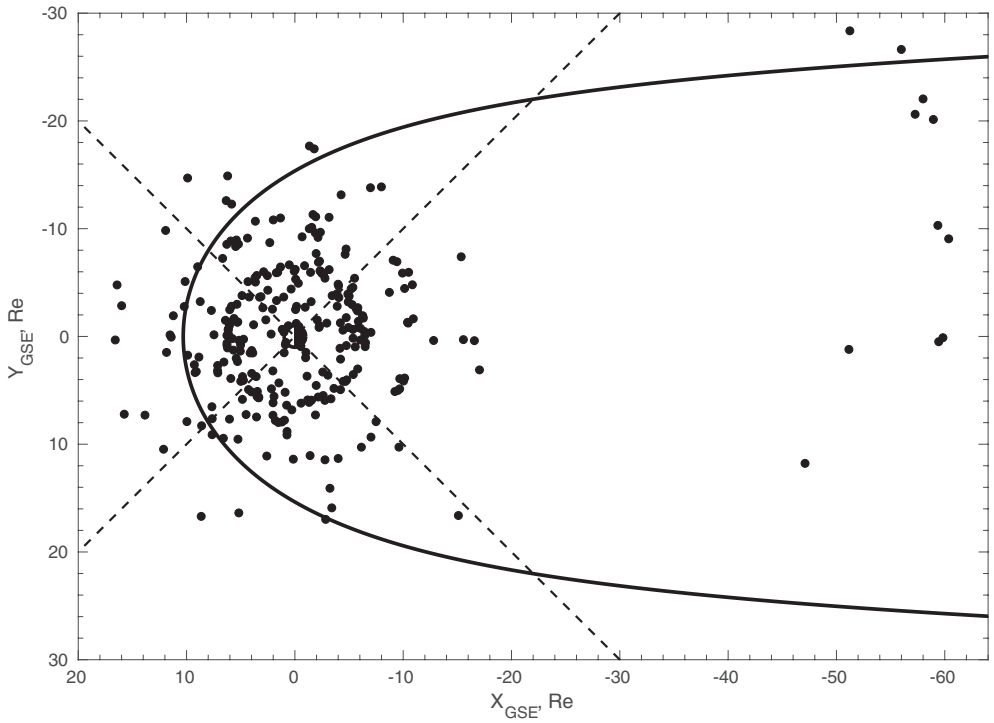

Figure 1. Satellite location during all the events. The dashed lines indicate four local times: midnight (21-03) LT, dawn (03-09) LT, noon (09-15) LT, dusk (15-21) LT. The magnetopause is drawn as reference using the model provided by Shue et al. (1998).

group all the observations together in order to improve the spatial coverage and to have a better view of the global magnetospheric response. Simultaneously, we individually analyzed the events to directly track the DPP response at different regions in space and ground. We then determined the Time-Of-Flight (TOF) difference between the DPP hitting the dayside magnetosphere and each of the satellites to estimate speed of propagation of the perturbation through the magnetosphere. We then determined arrival time differences between the DPP hitting the dayside magnetosphere and each of the satellites to estimate the propagation speed. The arrival of the DPP to the dayside magnetosphere is determined by the satellite located in the dayside with the largest X_{GSE} coordinate, or by time where SYM-H index suddenly increases in case there are no satellites located on the dayside. The main uncertainty of this method results from the events where the DPP arrival to the magnetosphere is computed with the SYM-H (1-min resolution), also the direction and inclination of the DPP plays an important role in the computed TOF. The speed of propagation in the antisunward direction can tell us if the signature observed is directly due to the DPP traveling at solar wind speed or if it is due to the propagation of MHD waves.

During each event, several individual satellite observations are made. In some cases, we group all the events in order in order to have a bigger number of single observations. In 82% of the individual satellite observations the arrival of the DPP compression to the satellite is observed as a step-like function. This is the main indicator being used in this study to establish the arrival of the magnetic compression to each satellite, which is used to compute the propagation speed in the antisunward direction. We also performed wavelet, and Fourier power-spectral-density (PSD) analysis of all satellite and ground-based observations. In order to make this possible we applied a high-pass filter to the magnetic field to try to reduce the impact of the step-like function component in the analysis. In the case of the PSD, we also divided the signal into two parts (before and after disturbance arrival) to detect ULF waves that are generated by the DPP. In both cases, the analysis was performed to detect waves in the Pc5 range.

In the case of the ground-based magnetometers, the 1-min resolution of the data limits the analysis capabilities of PSD. In addition, we divided each one of the magnetometer observations in two parts, one before

Table 1
Events Found Between 2007 and 2018 That Meet the Criteria Described in the Methodology section.

Event ID	Event date	IMF By	IMF Bz	IMF Bt	DPP speed	$\frac{\Delta P}{P}$	SI or SSC?
1	2011/02/18 01:30:00	0.9	4.0	5.7	−448	10.6	SSC
2	2011/06/05 05:55:00	−6.5	15.6	16.9	−544	2.8	N/A
3	2011/06/11 09:13:00	−4.5	6.0	7.6	−401	2.6	N/A
4	2011/08/04 21:53:20	−2.9	2.3	4.3	−398	4.0	SI
5	2011/10/05 07:36:37	3.8	3.4	5.2	−445	2.6	SI
6	2011/11/30 01:42:30	−3.2	5.8	6.9	−458	3.3	N/A
7	2012/01/24 15:00:05	−22.0	15.8	27.6	−625	7.6	SSC
8	2012/03/08 11:02:40	−0.3	9.2	10.4	−790	5.9	SSC
9	2012/04/23 03:20:20	5.8	1.3	5.9	−387	4.6	SSC
10	2012/05/21 19:35:35	−0.7	1.2	1.8	−388	3.2	SI
11	2013/01/19 17:32:00	2.3	2.9	4.6	−430	2.1	SI
12	2013/02/16 12:08:15	9.4	4.0	10.2	−388	2.0	SI
13	2013/03/18 06:12:00	−1.9	5.7	8.0	−572	1.6	N/A
14	2013/04/14 09:16:10	7.2	6.9	11.0	−520	1.3	N/A
15	2013/05/16 15:45:00	2.0	1.1	3.5	−410	1.4	N/A
16	2013/07/09 20:51:50	5.5	8.6	10.2	−415	3.4	SI
17	2013/12/01 13:07:20	1.8	7.2	8.2	−479	2.7	N/A
18	2013/12/13 13:23:00	−2.5	0.4	2.7	−320	2.8	SI
19	2014/01/09 20:10:20	−5.4	4.0	7.5	−460	3.2	SI
20	2014/03/20 10:16:30	−7.7	3.1	8.7	−347	1.6	N/A
21	2014/04/20 10:54:50	−0.6	8.2	8.3	−554	5.7	SSC
22	2014/05/03 17:47:15	−2.3	2.1	3.4	−330	1.4	SI
23	2014/06/07 16:51:45	−6.1	5.6	10.3	−420	4.7	SSC
24	2014/07/14 14:31:05	−1.9	8.3	8.9	−365	1.3	SI
25	2014/09/12 15:54:00	7.6	3.0	8.2	−600	9.1	SSC
26	2014/12/23 11:15:33	−11.5	3.3	13.5	−410	4.7	SI
27	2015/01/06 20:22:15	−3.8	7.7	8.6	−485	1.9	N/A
28	2015/01/07 06:16:00	1.8	7.4	7.9	−480	1.7	SSC
29	2015/03/17 04:44:00	10.7	15.6	19.0	−551	3.5	SSC
30	2015/03/31 08:32:10	−5.8	2.1	7.2	−360	2.3	SI
31	2015/06/25 05:30:00	−1.3	4.9	6.6	−652	1.4	N/A
32	2015/08/15 08:28:00	7.7	4.9	10.5	−450	2.2	SSC
33	2015/09/20 06:03:30	8.7	3.4	9.5	−498	2.3	SSC
34	2015/11/20 06:50:00	−4.6	2.2	5.3	−382	4.6	N/A
35	2017/07/02 20:53:30	−2.1	3.9	6.7	−435	1.1	N/A
36	2017/09/06 23:43:30	−3.4	2.5	4.7	−590	6.9	SSC
37	2017/11/25 00:33:55	2.5	4.4	5.4	−440	1.9	SI

IMF values are in nT and DPP speed in km/s.

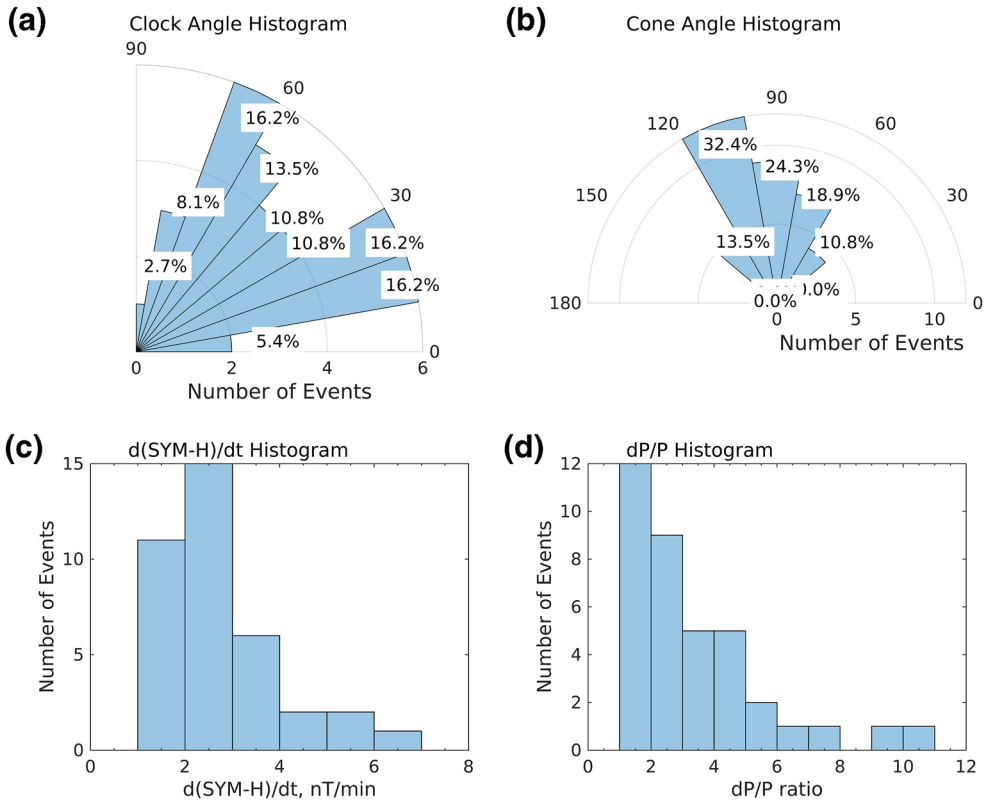

Figure 2. Event summary histograms. (a) Clock Angle. (b) Cone Angle. (c) d(SYM-H)/dt. (d) $\frac{\Delta P}{P}$.

the DPP arrival and one after the DPP arrival. We adjusted a third degree polynomial to each part and used it as reference to compute the root-mean-square-deviation (RMSD) which gives an estimation for the total amount of variability observed by the magnetometer as result of the DPP.

3. Event Characteristics

The solar wind and IMF conditions for the 37 DPP events are similar due to our selection criteria. All the events occur during northward IMF Bz, and all generate a compression in ground magnetometer data observed as an increase in SYM-H index over an average rise time of 6 min. Figure 2 summarizes the main characteristics of the events. The clock angle ($ar\cos\left(\frac{B_y}{\sqrt{\left(B_y^2+B_z^2\right)}}\right)$) is always between 0 and 90°, the cone angle ($ar\cos\left(\frac{B_x}{B}\right)$) is always between 40 and 140°.

The events are classified by the $\frac{\Delta P}{P}$ ratio and the events that had large pressure ratios also had large increases in SYM-H. The d(Sym-H)/dt mean is 2.7 nT/min and the median is 2.3 nT/min. This indicates that all large solar wind DPP during northward IMF have large compression signatures on the ground and are therefore ideal candidates to study the nonstorm-time magnetospheric response to rapid and large solar wind drivers. We compared our list of events with "Space Weather Database Of Notifications, Knowledge, Information" (DONKI) catalog (https://ccmc.gsfc.nasa.gov/donki/) and found that 18 of the events are CME impacting the Earth's magnetosphere. Based in "Observatori de l'Ebre" catalog (http://www.obsebre.es/en/), 13 of the events were sudden impulses, and 12 storm sudden commencements. However, the capability to take advantage of the big events finally depends on the amount and distribution of HSO satellites

throughout the magnetosphere. The next section presents one of the 37 events as "typical" best case example that highlights signatures seen in all the cases. The other events differ due to the location of the satellites and the size (dP/P) of the DPP, with smaller amplitude events have smaller magnetosphere and ionosphere signatures. Data and figures for all of the events are archived (see Appendix).

4. Event on September 6, 2017

In this section, we show one event as example of the 37 events analyzed. This event occurs at the beginning of a very active period of the Sun (Scolini et al., 2020), that developed geomagnetic storms and their effects in different regions of the magnetosphere. However, the immediate hours before this event were calm with northward IMF. At 23:43 UT an interplanetary shock driven by an ICME compressed the magnetosphere and generated magnetic perturbations which propagation we were able to track at different sectors and regions of the magnetosphere. Other events, especially the events with large dP/P ratios are very similar and therefore are not presented. However, figures are available in the data set deposited in Deep Blue which DOI number given in the Acknowledgment section.

For this event there are a total of six satellite missions (consisting of 12 satellites), 62 ground-based magnetometer stations (above 60° of magnetic latitude) with available data. For many of the events, Cluster, MMS and some of the THEMIS spacecraft travel very close to each other and therefore are treated as single observation points. However, in these circumstance the close spacecraft formations are used to assess propagation velocity. In this particular event, the spacecraft configuration allows the study of the global scale and also the small scale using Cluster and MMS. Figure 3a shows the location of the spacecraft constellation during this event. The magnetosphere structure is obtained with Tsyganenko T89 model, and the magnetopause is drawn using Shue et al. (1998) model. The solar wind OMNI data correspond to ACE and WIND data propagated to the bow shock and the propagation uncertainty depends of the solar wind conditions. In order to improve the estimation for the DPP arrival to the magnetopause, it was determined using the SYM-H index, the accuracy of the SYM-H for the arrival estimation of the DPP is higher than the OMNI data. Figures 3b–3f shows that the solar wind conditions previous to the DPP arrival are steady, the IMF Bz is constantly positive but low amplitude, and the solar wind flow speed is 480 km/s.

The propagation of the disturbance was tracked using the magnetic field instruments of each one of the spacecraft. Figure 4 shows the magnetic field magnitude of 11 spacecraft and the compression observed by each of them due to the propagation of the traveling magnetic cloud. The first plot shows the closest spacecraft to the Sun, while the last one shows the furthest spacecraft to the Sun. Note that a compression signature is observed at all spacecraft (except Cluster, explained below) and the timing of the observations are consistent with a signature propagation from the dayside magnetopause through the magnetosphere.

The first sign of the DPP arrival is given by the magnetospheric compression and wave activity observed by THEMIS-D $(11.5,0,-1.0)_{GSE}$ at 23:43:30 UT (shown in Figure 5), located at the dayside of the outer magnetosphere. The solar wind dynamic pressure before the DPP was around 0.9 nPa and the peak in the DPP was around 7.5 nPa $\frac{\Delta P}{P} \simeq 6.9$ and the IMF is $(2.0,-5.9,4.1)_{GSE} nT$, the solar wind flow speed observed by ACE is around 600 km/s, while WIND detects a flow speed of 580 km/s. The DPP induces an increase in SYM-H of 26 nT.

Dayside: The dayside response to the solar wind pressure pulse is observed by THEMIS-A, THEMIS-D, THEMIS-E, GOES-15, and Van Allen Probes. All of them observe the magnetic compression generated by the solar wind pressure pulse. THEMIS-D $(11.5,0,-1.0)_{GSE}$ is initially located on the magnetosphere side of the magnetopause and observes the compression as a couple of outbound discontinuity crossings. First, the spacecraft (Figure 5 crosses the magnetopause to the magnetosheath at 23:35 UT as result of a small increase in the solar wind dynamic pressure, later at 23:43:30 UT the spacecraft observes the compression of the magnetosheath and crosses the bow shock to enter the solar wind environment. Meanwhile, THEMIS-A $(6.5,2.4,0.3)_{GSE}$, THEMIS-E $(7.0,3.4,0.9)_{GSE}$ (shown in Figure 6), GOES-15 $(4.9,4.3,1.3)_{GSE}$, RBSP-A $(3.8,-1.0,-1.0)_{GSE}$ and RBSP-B $(5.6,1.4,0.2)_{GSE}$ are all located deeper in the magnetosphere. They observe similar compression signatures within 1 min of each other: an increase in the total magnetic field driven by the increase of the Bz component.

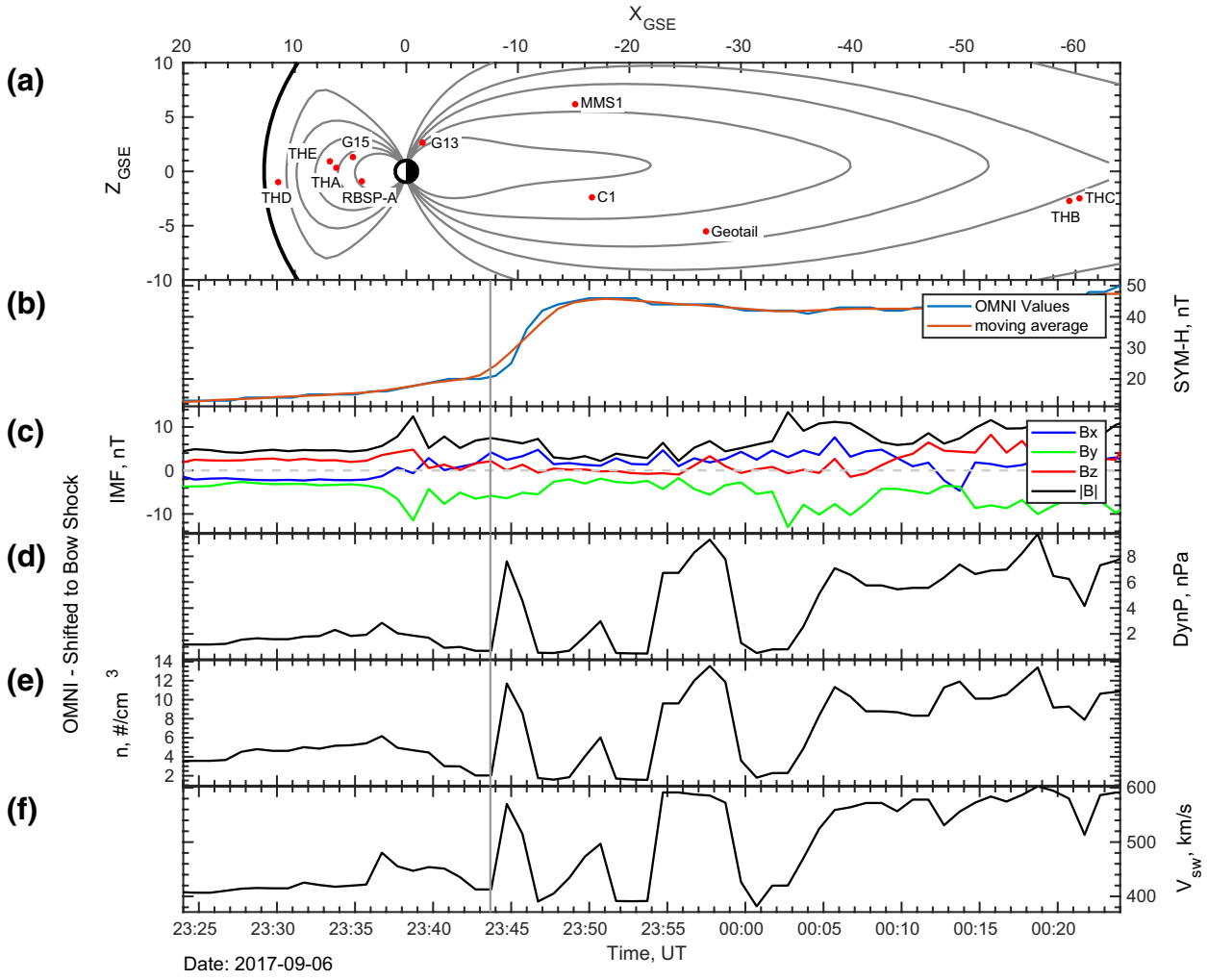

Figure 3. (a) XZ-Plane in GSE coordinates with the location of the spacecraft with Tsyganenko T89 as reference. The Magnetopause is drawn using the model provided by Shue et al. (1998). (b) SYM-H (nT) increases as result of the compression generated by the increase in the dynamic pressure. (c) IMF (nT) three components: Bx (blue), By (green), Bz (red), B total (black). (d) Solar wind dynamic pressure (nPa) shifted to the bow shock nose. (e) Solar wind number density (#/cm^3). (f) Solar wind flow speed (km/s).

Nightside: The nightside response is observed by Geotail, THEMIS-B, THEMIS-C, and the four Cluster spacecraft. The magnetic signature observed by Geotail $(-26.9,-12.8,-5.5)_{GSE}$ shows (see Figure 7) the DPP arrival as a tilt in the Bz component coinciding with a compression driven by By and Bz components. Further in the tail, THEMIS-B $(-59.4,-10.3,-2.7)_{GSE}$ shown in Figure 8 observes a signature proposed by Moldwin et al. (2001) as a Bz South-then-North turning previous to crossing the current sheet. THEMIS-C $(-60.4,-9.0,-2.5)_{GSE}$ shows an almost identical signature to THEMIS-B. Both signatures are also similar with Geotail despite the more than 33 Earth radii of separation. The average speed of the signal is computed using RBSP-B located on the dayside as reference point for the arrival of the DPP and the compression observed later by each satellite. The speed is computed by calculating the TOF, after identifying the DPP in the solar wind (start time) when possible and the compression observed by each one of the satellites available (end time). The computed speeds are 608, 623, 600 km/s for Geotail, THEMIS-B, and THEMIS-C respectively. These values are consistent with the solar wind speed observed by ACE (600 km/s) and WIND (580 km/s) during the DPP. Meanwhile, the Cluster spacecraft (Figure 9) located at $(-16.6,0.5,-2.5)_{GSE}$ observe a compression that is likely related to a previous process in the tail. This signature is probably result of a previous dynamic pressure increase such as the observed in Figure 3 at 23:37 UT, or to another process in the dynamics of the magnetosphere. The TOF computed speed for the signature is 1991 km/s, while the

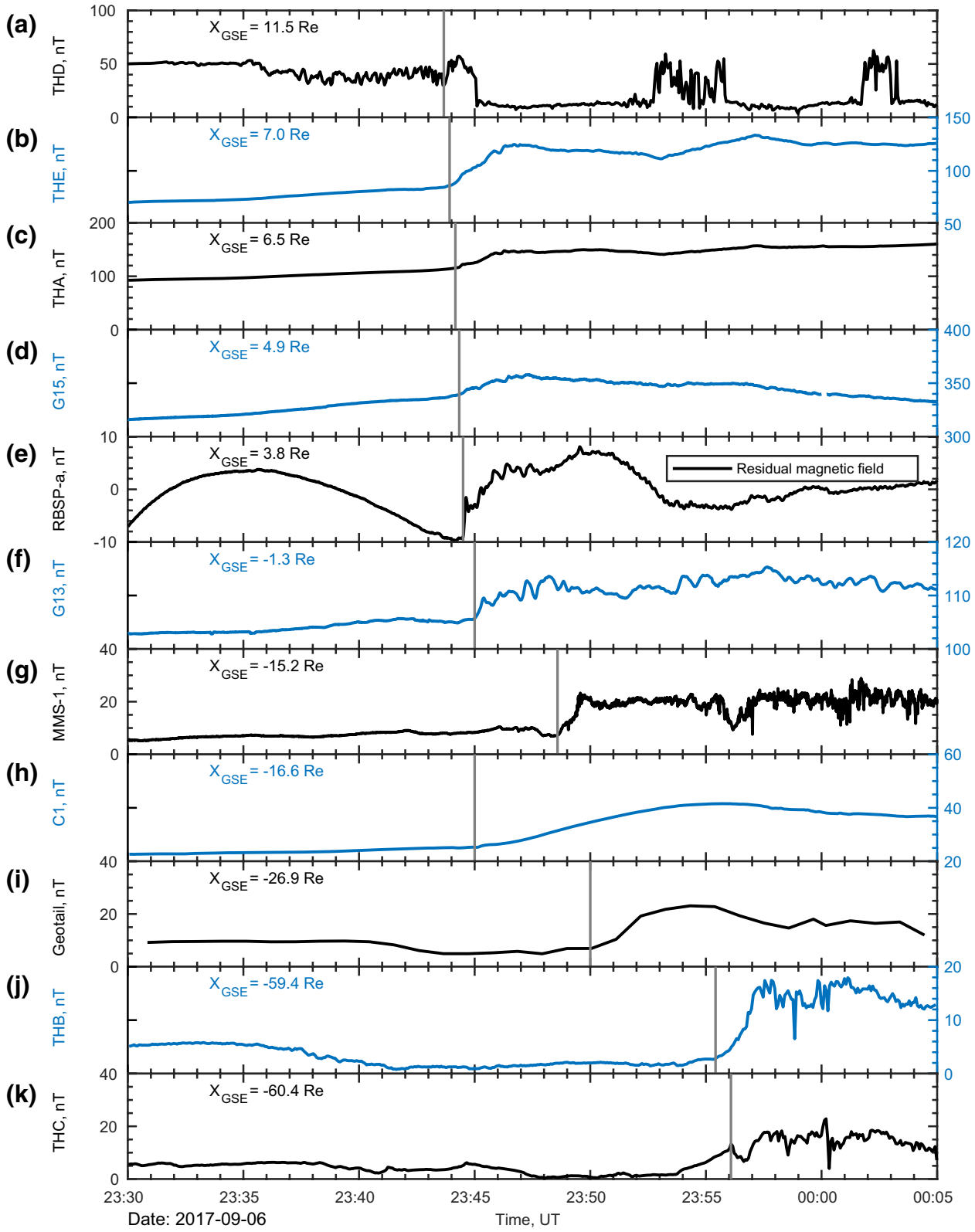

Figure 4. Magnetic field magnitude in nanoTesla as measured by multiple satellites. In the case of RBSP-a (plot (e)), the dipole component was subtracted using a fourth degree polynomial fitting.

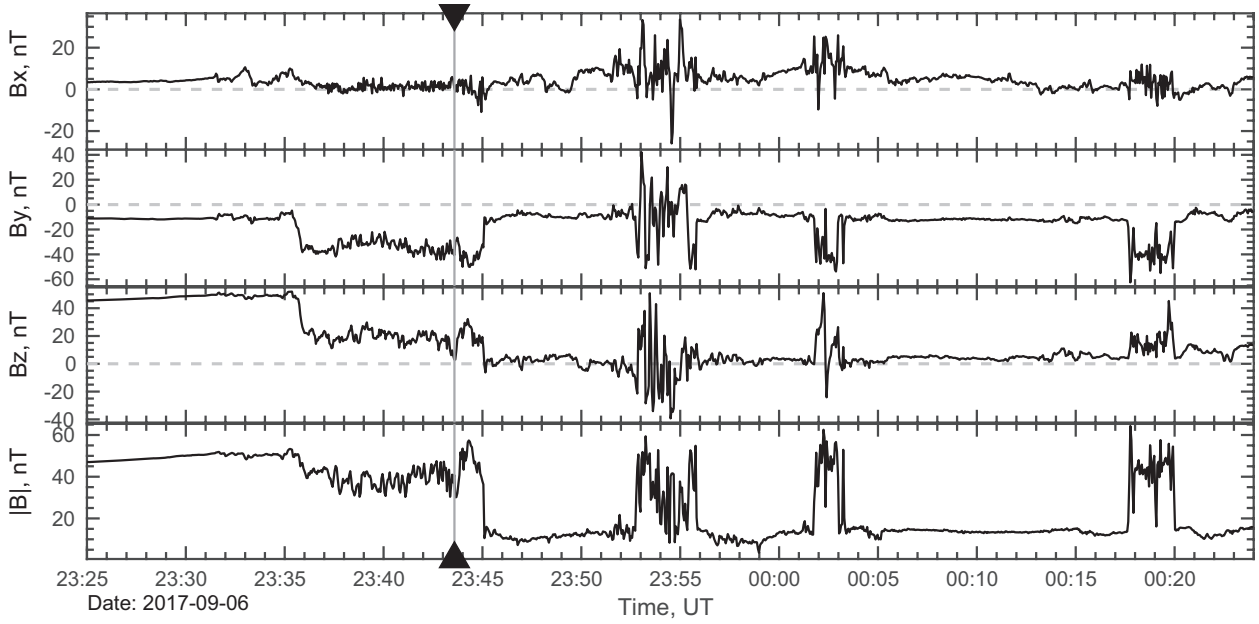

Figure 5. THD three magnetic field (nT) components and total magnetic field. THD is located at $(11.5,0,-1.0)_{GSE}$, it is the first satellite inside the magnetosphere to observe the compression. The inward movement of the magnetopause places THD in the solar wind at 23:43:30 UT. The triangles indicate the first detection of the DPP and the vertical line the DPP arrival, which in this case are the same.

TOF computed by cross correlation of the magnetic field magnitude measured by Cluster 2 and 3, show a tailward movement of 675 km/s in the X_{GSE}.

Dusk: While there are no satellites located in the inner magnetosphere dawn sector, there are five located in the dusk sector during this event. MMS spacecraft $(-15.2, 16.6, 6.2)_{GSE}$ magnetic field data are shown in Figure 10. The constellation travel in close formation and are considered a single observation. GOES-13 $(-1.3, 5.9, 2.6)_{GSE}$ shown in Figure 11 is located at the edge of dusk and night sectors of the inner magnetosphere,

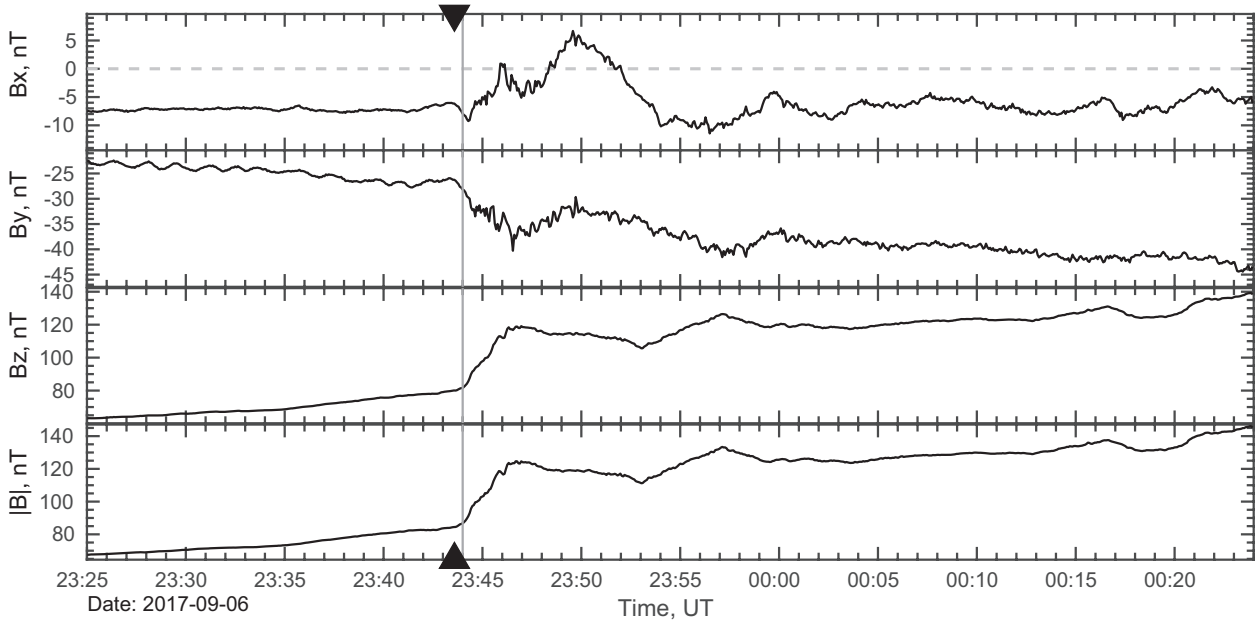

Figure 6. THE three magnetic field (nT) components and total magnetic field. THE is located at $(7.0,3.4,0.9)_{GSE}$ in the dayside magnetosphere, it observes a compression driven by the increase in the Bz. The triangles indicate the first detection of the DPP and the vertical line the DPP arrival to THE.

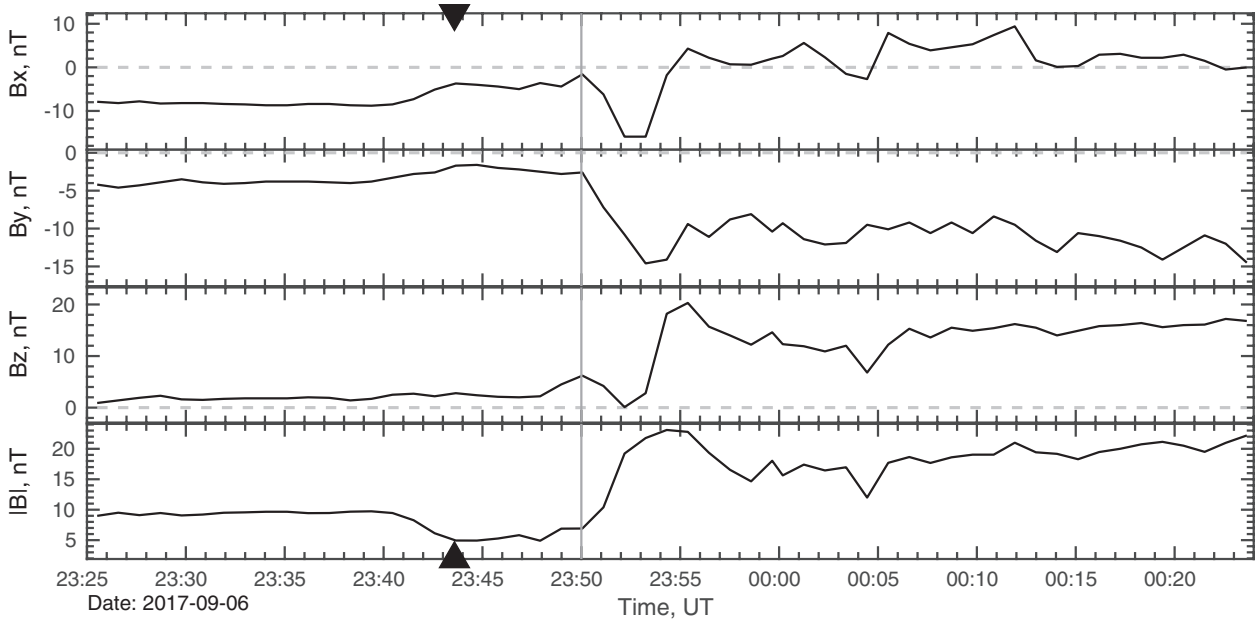

Figure 7. Geotail three magnetic field (nT) components and total magnetic field. Geotail is located at $(-26.9,-12.8,-5.5)_{GSE}$ near the neutral sheet, it observes a compression around 23:50 UT. The triangles indicate the first detection of the DPP and the vertical line the DPP arrival to Geotail. Data has only 1-min resolution.

observed the compression driven by an increase in the Bz component, and also ULF wave activity in all components. The MMS spacecraft located in the solar wind at dusk observed the DPP as outbound movement of the magnetopause and crossing to the magnetosheath. This is similar to the magnetopause motion proposed by D. D. Sibeck (1990) resulting from the magnetopause compression and generates a steep fast-mode wave in the magnetosphere that causes the magnetopause to flare outward.

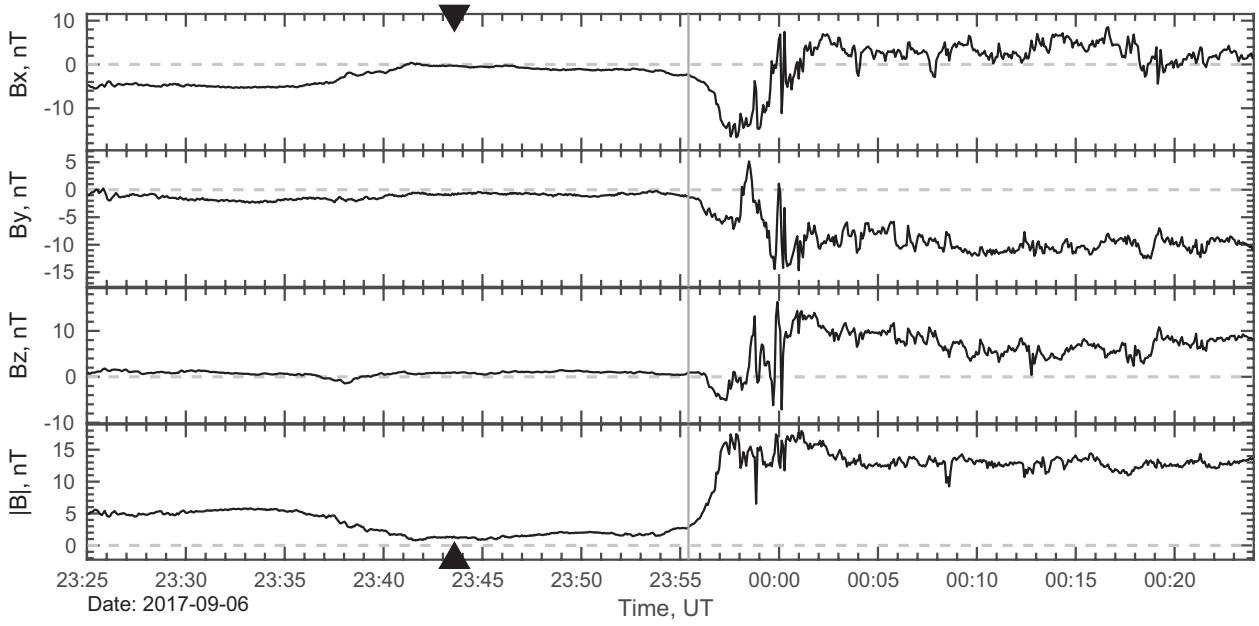

Figure 8. THB three magnetic field (nT) components and total magnetic field. THB is located at $(-59.4,-10.3,-2.7)_{GSE}$ very close to the neutral sheet. The triangles indicate the first detection of the DPP and the vertical line the DPP arrival to THB.

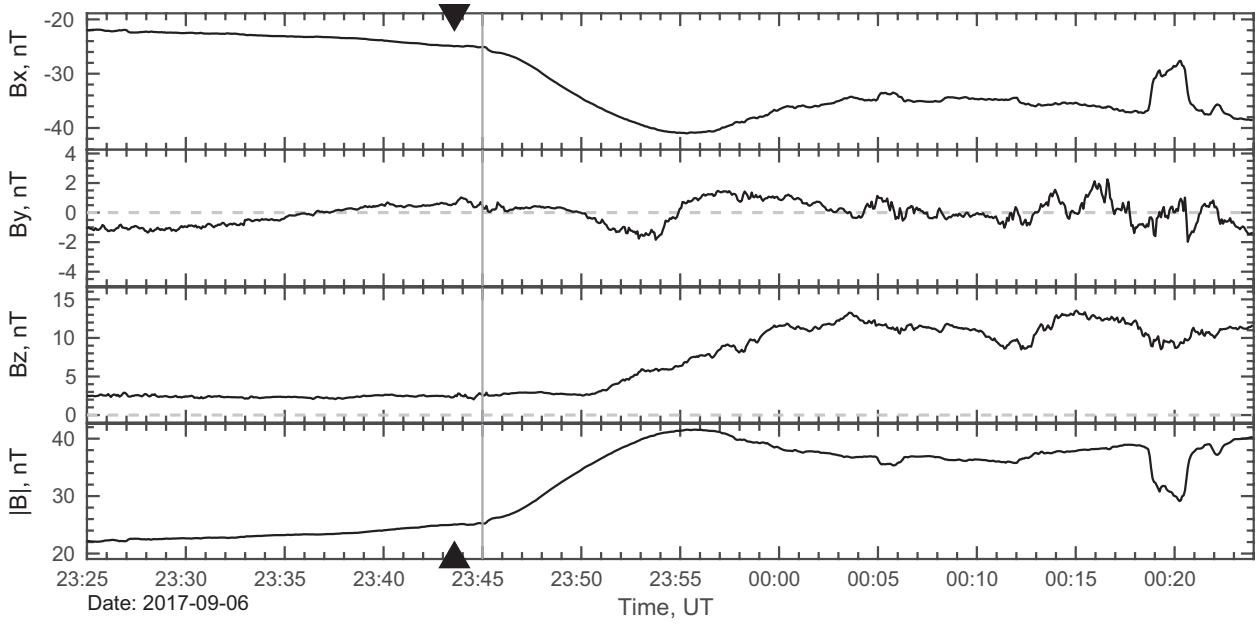

Figure 9. Cluster-1 three magnetic field (nT) components and total magnetic field. Cluster-1 is located at $(-16.6, 0.5, -2.5)_{GSE}$ in the southern tail lobe, at these locations the compressions are commonly driven Bx. The triangles indicate the first detection of the DPP and the vertical line the DPP arrival to Cluster-1.

Ground-Based Magnetometers: We observed the magnetic field variations between the periods before and after the DPP arrival. The top panel of Figure 12 shows Ministik Lake magnetometer station as example. In average, the magnetic field magnitude increase 33 nT after the DPP arrival, which is also observed by the SYM-H index increase. We also performed a magnetic field variability analysis to examine the effect of the DPP as observed on the ground. We adjusted third degree polynomials for the periods of time before and after the DPP arrival (see Figure 12). We computed the RMSD to obtain a measurement of the variability of the signal. For this event, 61 of 62 stations observed an increase of the magnetic field variability after the

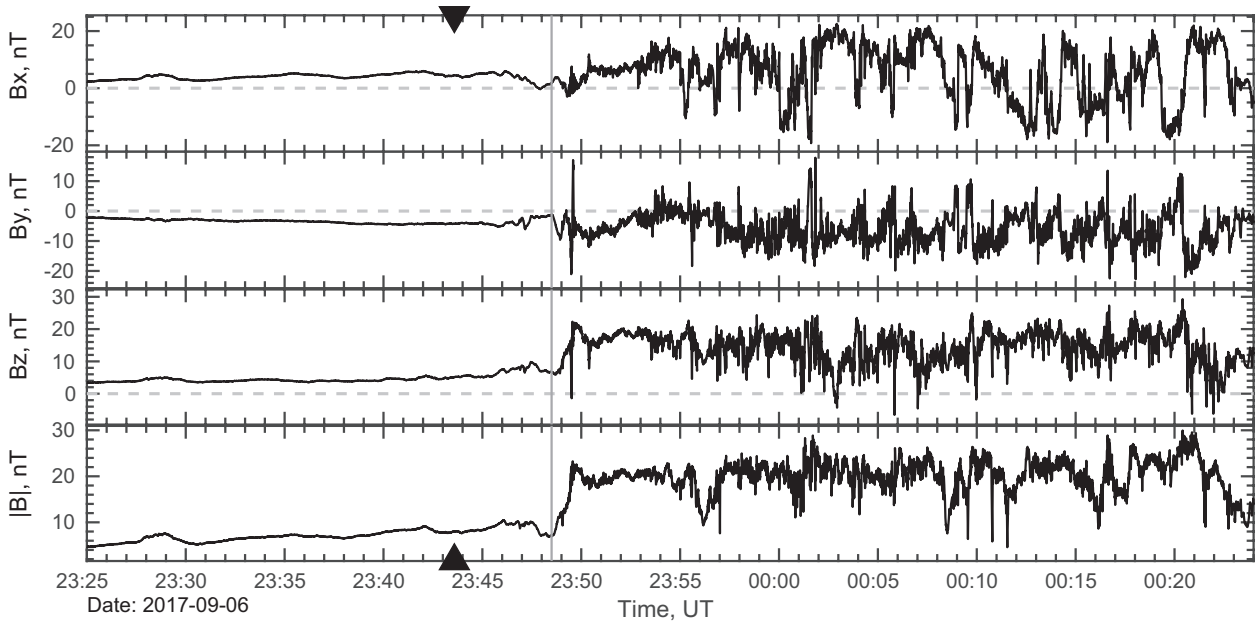

Figure 10. MMS-1 three magnetic field (nT) components and total magnetic field. MMS-1 is located at $(-15.2,16.6,6.2)_{GSE}$ near the plasmasheet in the dusk flank of the magnetotail. An increase in the magnetic field magnitude is observed at 23:48:30 UT. The triangles indicate the first detection of the DPP and the vertical line the DPP arrival to MMS-1.

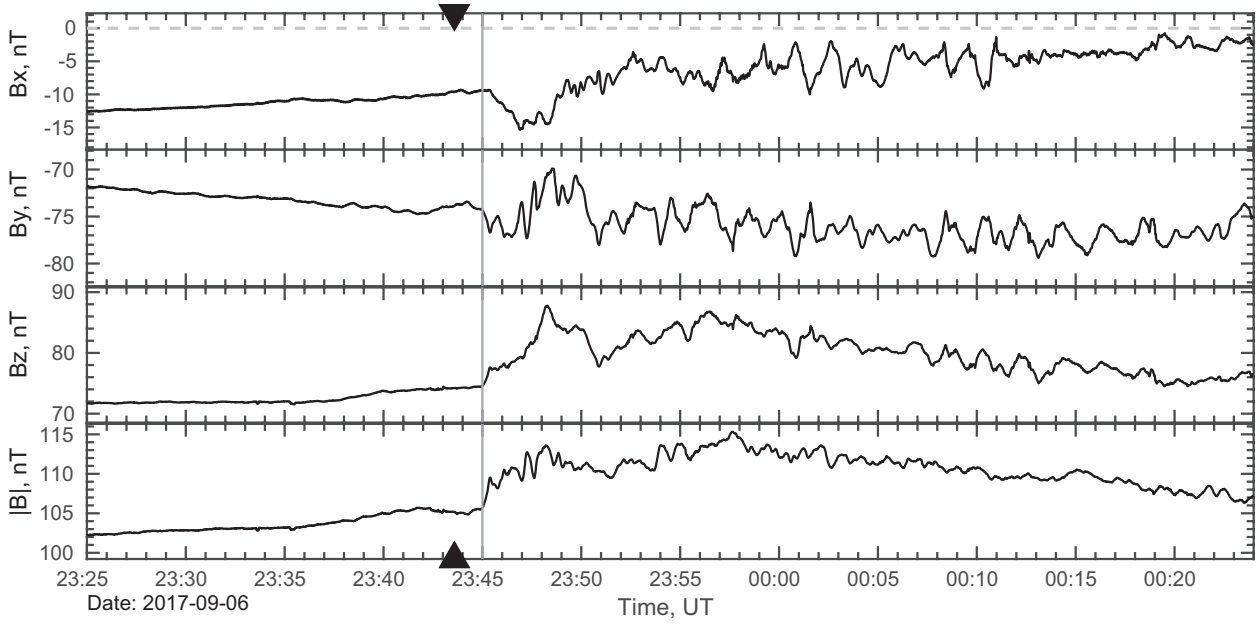

Figure 11. G13 three magnetic field (nT) components and total magnetic field. GOES-13 is located at $(-1.3,5.9,2.6)_{GSE}$. The triangles indicate the first detection of the DPP and the vertical line the DPP arrival to GOES-13.

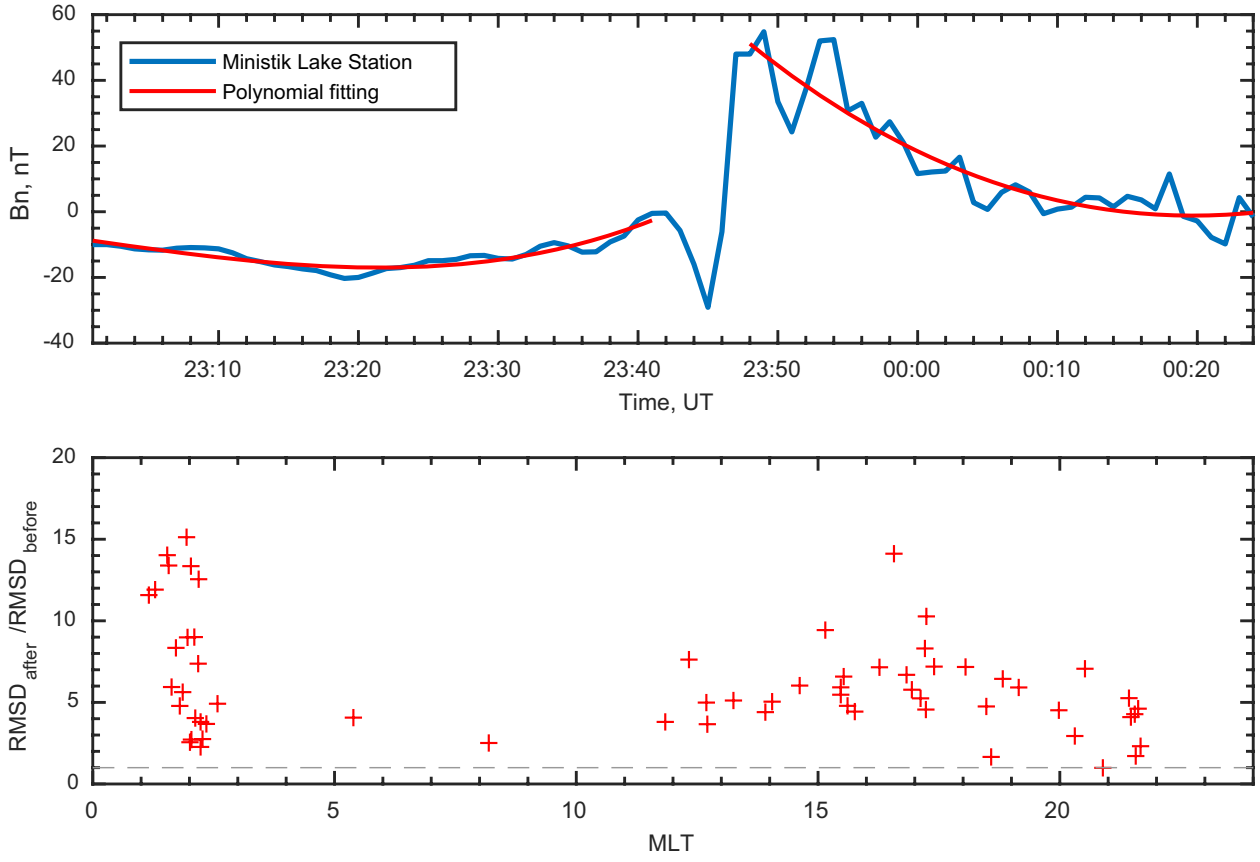

Figure 12. Top: As example, Ministik Lake station magnetogram after removing daily baseline in blue. Polynomial fitting by least squares for times before and after the DPP disturbance arrival. Bottom: ratio of the root-mean-square-deviation after and before the DPP disturbance arrival as function of magnetic local time for all stations.

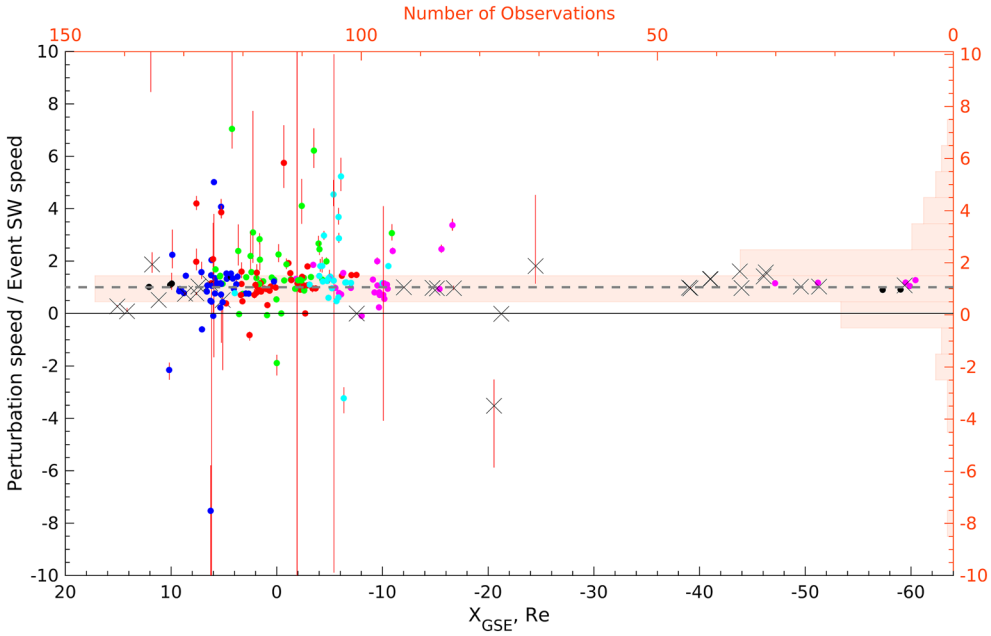

Figure 13. Transient speed measured by Time-Of-Flight between several spacecraft for each event as function of the solar wind speed during that event. Error bars are defined as the error generated during the identification of the time of a magnetic perturbation that can be associated to the DPP propagation. The color of the dots represents the region where the satellite was located. Solar wind: black crosses; day sector inner magnetosphere: blue; dawn sector inner magnetosphere green; dusk sector inner magnetosphere: red; night sector inner magnetosphere: cyan; tail lobes: magenta; magnetosheath (around any region): black dots.

DPP arrival. The mean RMSD before the DPP arrival was 9.72 nT, the mean RMSD after the DPP arrival was 48.7 nT.

5. Results

The events detected in this study show systematic behavior of the magnetosphere perturbation due to the antisunward movement of the DPPs outside the magnetosphere. We are able to follow the tailward propagation using different satellites at multiple locations of the magnetosphere. In 27 of the events, there are observations available near or inside geostationary orbit, in 25 of the events there is at least one satellite observing signatures corresponding to the onset of the ULF waves, probably related to the magnetospheric oscillation modes triggered by the DPP. However, in most of the cases, the signatures detected are a direct result of the DPP compression through the boundaries of the magnetosphere, which impact the magnetosphere in different ways depending on the region and local time sector.

We are able to identify these signatures using different spacecraft that observe a magnetic compression. In Figure 13 the TOF V_{xGSE} speed of tracked signatures is shown with respect to the X_{GSE} coordinate. The arrival time is obtained by visual inspection and the error bars correspond to uncertainties due to the data time resolution and noise that can compromise the correct identification of the exact arrival time. Figure 13 shows that the speed computed in 209 of 229 observations was between the standard deviation of the distribution of TOF and the respective solar wind speed of each event. The reason why higher than solar wind speeds are observed in the dayside is probably due to the compressional fast-mode wave generated by the DPP as described by Tamao (1964), which could be easily mistaken with the compression generated by the propagating DPP moving tailward. We suggest that the dispersion of the perturbation speeds (specially, those outside the standard deviation) is mainly due to the inclination of the DPP front, as we observed in six events where multispacecraft timing was available in the solar wind. When the inclination in one dimension of the DPP front is considerably larger in relation to the separation of the satellites in the same dimension, the separation becomes important and explains the discrepancies between the perturbation speed expected and computed by TOF. For example, if two satellites have a separation of 10 Re only in the

Y_{GSE} component, a DPP front traveling at 400 km/s and an inclination of 45° with respect to dawn and dusk, the two satellites will observe a delay between them of 160 s equivalent to 10 Re. The computed speeds of the DPP are outside realistic propagation wave speeds in several of the observations: in 3.5% of observations the computed speed is higher than the Alfvénic speed at any region of the magnetosphere, and in a 7% of the observations there were negatives values (i.e. implying moving sunward) were found.

A survey of the type of response observed was made for all in space observations collected during the 37 events. The inner magnetosphere response analysis was made using GOES-13 and GOES-15. The results show that in the inner magnetosphere, the magnetic compression is mainly driven by the Bz component of the local magnetic field, and the compression is observed in all local time sectors. We used FFT analysis to study the Pc4-5 waves power. We separated the observations into before and after the compression, in order to avoid the power generated by the step-like function due to the compression. The results show an increase in power in at least one of the magnetic field components in 86% of the observations and in 73% of the events. The increase in Pc4-5 wave power in at least one of the magnetic field components was observed in all the dayside (09-15 LT) observations, 81% in the dawn (03-09 LT) sector, 80% in the dusk (15-21 LT) sector, and 86% in the night (21-03) sector. From the point of view of the ground-based magnetometers. Due to their low time resolution (1-min), it is not possible to track the signal between different stations, or perform an FFT analysis for the Pc4-Pc5 range, but it is possible to observe the compression generated by the DPP, and the increase in the variability generated by the DPP. Counting all the ground-based magnetometer stations available during the 37 events, the magnetometers performed 2,486 time series of observations. In 2071, time series there was an increase in the magnetic field after the arrival of the DPP, equivalent to the 83% of all observations. A total of 2,194, equivalent to a 88% showed an increase in the magnetic field RMSD. On average, the RMSD increase significantly (5.8 times) after the DPP arrival.

6. Discussion

We use the Heliophysics System Observatory to perform a global view of the magnetospheric response to sudden increases in the solar wind dynamic pressure during northward IMF. The conditions set for event detection, favored the detection of events with of large DPP during quiet conditions. The current capabilities of the HSO make possible simultaneous observation and tracking of dynamic pressure pulses from the solar wind through most of the magnetospheric cavity. The tracking of perturbation can offer a more complete explanation to many single event studies or statistical studies from single satellite missions made in the past especially enabling the observation of propagating signatures.

The results show the importance of observing the magnetosphere from multiple satellites throughout the magnetosphere. The analyzed events show different types of magnetic signals, such as dayside compressions, ULF waves at dawn, dusk and night sectors, and in the magnetotail. There was also observations of South-then-North compression signatures in the magnetotail. This work examined the DPP signatures traveling with the solar wind while compressing the magnetosphere from upstream to the magnetotail. While the initial impact of the DPP into the magnetosphere triggers fast-mode waves that propagate faster than the solar wind, the main transients observed travel at solar wind speed around the magnetopause and generate new ULF signatures.

We found that the tracking becomes very complicated to perform when the satellites are located in the inner magnetosphere. MHD waves resulting from the compression move faster and along different paths. However, in the case of the tail the situation is more clear. The magnetic lobe field pressure increases as it balances with the static and dynamic pressure as stated by Fairfield and Jones (1996) and Collier et al. (1998). Our results are in agreement with Huttunen et al. (2005) that SIs in the tail move at solar wind speed. Moldwin et al. (2001) showed that a short period (1–10 min) DPP traveling tailward through the magnetosphere can be seen as South-then-North Bz signatures. However, the DPPs involved in our study have longer duration (above 20 min) and therefore we observed only the first half of the south-then-north Bz signature.

We found that the magnetic response at geosynchronous orbit is a sudden increase in the magnetic field magnitude. This is in agreement with observations reported by Borodkova et al. (2005, 2008), and Zuo et al. (2015). It is also found that the perturbation is moving at solar wind speed, which is in agreement with the SIs speed reported by Huttunen et al. (2005) using Cluster observations in the tail. Our study using

the HSO is able to clearly observe the propagation of the DPP signatures throughout the magnetosphere essentially knitting together the earlier studies that were limited to specific regions of the magnetosphere.

In relation to the unrealistic inferred velocities (such as negatives propagation speed), Oliveira et al. (2018) and Oliveira and Raeder (2015), found fast moving shocks tend to have smaller inclination angle than slower shocks. When comparing the computed DPP speeds with the solar wind speed of each event, it was found that the outlier values correspond mainly to slow solar wind, which would suggest that those values were from DPP fronts with high inclination with respect to the X_{GSE} coordinate.

7. Conclusions

Large DPP give rise to systematic signatures through all regions and sectors of the magnetosphere. In addition to the waves propagating inside the magnetospheric cavity, the increase in the dynamic pressure in the solar wind creates a disturbance that propagates tailward through the magnetosphere at speeds close to the solar wind speed, the disturbance can be tracked using the satellites that form the Heliophysics System Observatory. The assumption of a planar solar wind disturbance explains the majority of the events studied here. However, the differences in plasma density in different regions, and the angle of the disturbance front generates discrepancies in the calculated propagation velocities. The analysis of the disturbance angle explained the differences in six of the events where multispacecraft timing was possible to perform due to the Cluster mission location in the solar wind.

Many of the events identified in this study lend themselves to deeper analysis due to having multiple observations in specific regions (opposed to distributed in multiple regions as focused upon here) enabling studies examining smaller scales. A future study is analyzing recently available 1-s resolution ground-based magnetometer data from SuperMag, and Intermagnet. For example, we selected some of the events studied here to observe the DPPs' propagation effects in the inner magnetosphere. We will focus in the propagation of the preliminary impulse from geostationary orbit altitude to the Earth's surface, including its speed and polarity dependence with latitude and local time, to evaluate the different theories about its propagation, which we expect will contribute to improved understanding of the global dynamics of the magnetosphere.

Appendix A: Data

In order to facilitate reproducibility, all the data collected for this study, including the data used for the figures were uploaded to the data service from University of Michigan, *Deep Blue* with the doi: https://doi.org/10.7302/keks-rg16. All the data collected were transformed into ASCII format. The data corresponds to observations of the solar wind, magnetosphere and at Earth's surface for all 37 events analyzed for this study. The solar wind observations consist in magnetic field, density, and velocity observations. The magnetosphere observations consist of magnetic field observations from all the satellites. The Earth's surface observations consist of magnetic field observations from ground-based magnetometer. For each time series of measurements there is a plot of such time series.

Data Availability Statement

Acknowledgments
The authors acknowledge the support of this study by NSF AGS 1654044, 1450512, and by the Comisión Nacional de Desarrollo Científico y Tecnológico of Chile. The authors also acknowledge to the SuperMAG collaborators (http://supermag.jhuapl.edu/). The authors acknowledge Arturo Lopez from the University of Michigan for helping us review catalogs of sudden impulses and sudden storm commencements. The authors also thank to the Observatori de l'Ebre (http://www.obsebre.es/en/rapid) for their catalog of sudden impulses and sudden storm commencements.

The authors also thank the Space Physics Data Facility, NASA for IMF data and MMS, THEMIS, Cluster, Van Allen probes and Geotail data obtained from the CDAWeb (https://cdaweb.gsfc.nasa.gov/), and the "Space Weather Database Of Notifications, Knowledge, Information (DONKI)" catalog (https://kauai.ccmc.gsfc.nasa.gov/DONKI/search/). Finally, the authors also thank to the National Centers for Environmental Information for the GOES data available in (https://www.ngdc.noaa.gov/stp/satellite/goes/). The authors thank to the Deep Blue data service from the University of Michigan for providing a repository where the data of this study was uploaded (DOI: https://doi.org/10.7302/keks-rg16).

References

Ables, S. T., & Fraser, B. J. (2005). Observing the open-closed boundary using cusp-latitude magnetometers. *Geophysical Research Letters*, *32*(10). https://doi.org/10.1029/2005GL022824

Angelopoulos, V. (2009). The themis mission. *Space Science Reviews*, *141*(1–4), 5–34. https://doi.org/10.1007/s11214-008-9336-1

Araki, T. (1977). Global structure of geomagnetic sudden commencements. *Planetary and Space Science*, *25*(4), 373–384. https://doi.org/10.1016/0032-0633(77)90053-8

Archer, M., Horbury, T., Eastwood, J., Weygand, J., & Yeoman, T. (2013). Magnetospheric response to magnetosheath pressure pulses: A low-pass filter effect. *Journal of Geophysical Research*, *118*(9), 5454–5466. https://doi.org/10.1002/jgra.50519

Borodkova, N., Liu, J., Huang, Z., & Zastenker, G. (2008). Geosynchronous magnetic field response to the large and fast solar wind dynamic pressure change. *Advances in Space Research*, *41*(8), 1220–1225. https://doi.org/10.1016/j.asr.2007.05.075

Borodkova, N., Zastenker, G., Riazantseva, M., & Richardson, J. (2005). Large and sharp solar wind dynamic pressure variations as a source of geomagnetic field disturbances at the geosynchronous orbit. *Planetary and Space Science*, *53*(1–3), 25–32. https://doi.org/10.1016/j.pss.2004.09.025

Chi, P., & Russell, C. (2005). Travel-time magnetoseismology: Magnetospheric sounding by timing the tremors in space. *Geophysical Research Letters*, *32*(18). https://doi.org/10.1029/2005GL023441

Chi, P., Russell, C., Raeder, J., Zesta, E., Yumoto, K., Kawano, H., et al. (2001). Propagation of the preliminary reverse impulse of sudden commencements to low latitudes. *Journal of Geophysical Research*, *106*(A9), 18857–18864. https://doi.org/10.1029/2001JA900071

Claudepierre, S., Hudson, M., Lotko, W., Lyon, J., & Denton, R. (2010). Solar wind driving of magnetospheric ulf waves: Field line resonances driven by dynamic pressure fluctuations. *Journal of Geophysical Research*, *115*(A11). https://doi.org/10.1029/2010JA015399

Collier, M., Slavin, J., Lepping, R., Ogilvie, K., Szabo, A., Laakso, H., & Taguchi, S. (1998). Multispacecraft observations of sudden impulses in the magnetotail caused by solar wind pressure discontinuities: Wind and imp 8. *Journal of Geophysical Research*, *103*(A8), 17293–17305. https://doi.org/10.1029/97JA02870

Dungey, J. W. (1961). Interplanetary magnetic field and the auroral zones. *Physical Review Letters*, *6*(2), 47–48. https://doi.org/10.1103/PhysRevLett.6.47

Elkington, S. R., Hudson, M. K., & Chan, A. A. (1999). Acceleration of relativistic electrons via drift-resonant interaction with toroidal-mode pc-5 ulf oscillations. *Geophysical Research Letters*, *26*(21), 3273–3276. https://doi.org/10.1029/1999GL003659

Fairfield, D., & Jones, J. (1996). Variability of the tail lobe field strength. *Journal of Geophysical Research*, *101*(A4), 7785–7791. https://doi.org/10.1029/95JA03713

Huttunen, K., Slavin, J., Collier, M., Koskinen, H., Szabo, A., Tanskanen, E., et al. (2005). Cluster observations of sudden impulses in the magnetotail caused by interplanetary shocks and pressure increases. *Annales Geophysicae*, *23*(2), 609–624. https://doi.org/10.5194/angeo-23-609-2005

Kataoka, R., Fukunishi, H., Lanzerotti, L., Rosenberg, T., Weatherwax, A., Engebretson, M., & Watermann, J. (2002). Traveling convection vortices induced by solar wind tangential discontinuities. *Journal of Geophysical Research*, *107*(A12), SMP–22-1–SMP–22-12. https://doi.org/10.1029/2002JA009459

Kokubun, S. (1983). Characteristics of storm sudden commencement at geostationary orbit. *Journal of Geophysical Research*, *88*(A12), 10025–10033. https://doi.org/10.1029/JA088iA12p10025

Konik, R., Lanzerotti, L., Wolfe, A., Maclennan, C., & Venkatesan, D. (1994). Cusp latitude magnetic impulse events: 2. interplanetary magnetic field and solar wind conditions. *Journal of Geophysical Research*, *99*(A8), 14831–14853. https://doi.org/10.1029/93JA03241

Lanzerotti, L., Konik, R., Wolfe, A., Venkatesan, D., & Maclennan, C. (1991). Cusp latitude magnetic impulse events: 1. occurrence statistics. *Journal of Geophysical Research*, *96*(A8), 14009–14022. https://doi.org/10.1029/91JA00567

Lanzerotti, L., Wolfe, A., Trivedi, N., Maclennan, C., & Medford, L. (1990). Magnetic impulse events at high latitudes: Magnetopause and boundary layer plasma processes. *Journal of Geophysical Research*, *95*(A1), 97–107. https://doi.org/10.1029/JA095iA01p00097

Lee, D.-Y., & Lyons, L. (2004). Geosynchronous magnetic field response to solar wind dynamic pressure pulse. *Journal of Geophysical Research*, *109*(A4). https://doi.org/10.1029/2003JA010076

Moldwin, M. B., Collier, M. R., Slavin, J. A., & Szabo, A. (2001). On the origin of reverse polarity tcrs. *Geophysical Research Letters*, *28*(10), 1925–1928. https://doi.org/10.1029/2000GL012485

Moldwin, M. B., & Hughes, W. J. (1994). Observations of earthward and tailward propagating flux rope plasmoids: Expanding the plasmoid model of geomagnetic substorms. *Journal of Geophysical Research*, *99*(A1), 183–198. https://doi.org/10.1029/93JA02102

Nishida, A. (1983). Imf control of the earth's magnetosphere, *Space Science Reviews*, *34*, 185–200. https://doi.org/10.1007/BF00194626

Oliveira, D., Arel, D., Raeder, J., Zesta, E., Ngwira, C., Carter, B., et al. (2018). Geomagnetically induced currents caused by interplanetary shocks with different impact angles and speeds. *Space Weather*, *16*(6), 636–647. https://doi.org/10.1029/2018SW001880

Oliveira, D., & Raeder, J. (2015). Impact angle control of interplanetary shock geoeffectiveness: A statistical study. *Journal of Geophysical Research: Space Physics*, *120*(6), 4313–4323. https://doi.org/10.1002/2015JA021147

Petrinec, S., & Russell, C. (1993). An empirical model of the size and shape of the near-earth magnetotail. *Geophysical Research Letters*, *20*(23), 2695–2698. https://doi.org/10.1029/93GL02847

Rew, R., & Davis, G. (1990). Netcdf: An interface for scientific data access. *IEEE Computer Graphics and Applications*, *10*(4), 76–82. https://doi.org/10.1109/38.56302

Russell, C., & Ginskey, M. (1993). Sudden impulses at low latitudes: Transient response. *Geophysical Research Letters*, *20*(11), 1015–1018. https://doi.org/10.1029/93GL01257

Russell, C., & Ginskey, M. (1995). Sudden impulses at subauroral latitudes: Response for northward interplanetary magnetic field. *Journal of Geophysical Research*, *100*(A12), 23695–23702. https://doi.org/10.1029/95JA02495

Russell, C., Ginskey, M., & Petrinec, S. (1994). Sudden impulses at low-latitude stations: Steady state response for northward interplanetary magnetic field. *Journal of Geophysical Research*, *99*(A1), 253–261. https://doi.org/10.1029/93JA02288

Sanny, J., Tapia, J., Sibeck, D., & Moldwin, M. (2002). Quiet time variability of the geosynchronous magnetic field and its response to the solar wind. *Journal of Geophysical Research*, *107*(A12), SMP16-1–SMP16-10. https://doi.org/10.1029/2002JA009448

Scolini, C., Chané, E., Temmer, M., Kilpua, E. K., Dissauer, K., Veronig, A. M., et al. (2020). Cme–cme interactions as sources of cme geoeffectiveness: The formation of the complex ejecta and intense geomagnetic storm in 2017 early september. *The Astrophysical Journal Supplement Series*, *247*(1), 21–27. https://doi.org/10.3847/1538-4365/ab6216

Shue, J.-H., Song, P., Russell, C., Steinberg, J., Chao, J., Zastenker, G., et al. (1998). Magnetopause location under extreme solar wind conditions. *Journal of Geophysical Research*, *103*(A8), 17691–17700. https://doi.org/10.1029/98JA01103

Sibeck, D. (1990). A model for the transient magnetospheric response to sudden solar wind dynamic pressure variations. *Journal of Geophysical Research*, *95*(A4), 3755–3771. https://doi.org/10.1029/JA095iA04p03755

Sibeck, D. G., Lopez, R., & Roelof, E. (1991). Solar wind control of the magnetopause shape, location, and motion. *Journal of Geophysical Research*, *96*(A4), 5489–5495. https://doi.org/10.1029/90JA02464

Singer, H., Matheson, L., Grubb, R., Newman, A., & Bouwer, D. (1996). Monitoring space weather with the goes magnetometers. In: *Goes-8 and beyond*. Proceedings of the SPIE, Vol. 2812, 299–308. https://doi.org/10.1117/12.254077

Slinker, S., Fedder, J., Hughes, W., & Lyon, J. (1999). Response of the ionosphere to a density pulse in the solar wind: Simulation of traveling convection vortices. *Geophysical Research Letters*, *26*(23), 3549–3552. https://doi.org/10.1029/1999GL010688

Spence, H. E., Reeves, G., Baker, D., Blake, J., Bolton, M., Bourdarie, S., et al. (2013). Science goals and overview of the radiation belt storm probes (rbsp) energetic particle, composition, and thermal plasma (ect) suite on NASA's van allen probes mission. *Space Science Reviews*, *179*(1–4), 311–336. https://doi.org/10.1007/s11214-013-0007-5

Takahashi, K., & Ukhorskiy, A. Y. (2007). Solar wind control of pc5 pulsation power at geosynchronous orbit. *Journal of Geophysical Research*, *112*(A11). https://doi.org/10.1029/2007JA012483

Tamao, T. (1964). The structure of three-dimensional hydromagnetic waves in a uniform cold plasma. *Journal of Geomagnetism and Geoelectricity*, *16*(2), 89–114. https://doi.org/10.5636/jgg.16.89

Taylor, H. E. (1969). Sudden commencement associated discontinuities in the interplanetary magnetic field observed by imp 3. *Solar Physics*, *6*(2), 320–334. https://doi.org/10.1007/BF00150957

Trattner, K., Mulcock, J., Petrinec, S., & Fuselier, S. (2007). Probing the boundary between antiparallel and component reconnection during southward interplanetary magnetic field conditions. *Journal of Geophysical Research*, *112*(A8). https://doi.org/10.1029/2007JA012270

Troitskaya, V., & Bolshakova, O. (1988). Diagnostics of the magnetosphere using multipoint measurements of ulf-waves. *Advances in Space Research*, *8*(9–10), 413–425. https://doi.org/10.1016/0273-1177(88)90155-X

Tsurutani, B. T., & Gonzalez, W. (1995). The efficiency of "viscous interaction" between the solar wind and the magnetosphere during intense northward imf events. *Geophysical Research Letters*, *22*(6), 663–666. https://doi.org/10.1029/95GL00205

Usanova, M., Mann, I., Bortnik, J., Shao, L., & Angelopoulos, V. (2012). Themis observations of electromagnetic ion cyclotron wave occurrence: Dependence on ae, symh, and solar wind dynamic pressure. *Journal of Geophysical Research*, *117*(A10). https://doi.org/10.1029/2012JA018049

Yao, L., Zuo, P., Feng, X., & Liu, Z. (2010). Responses of the magnetotail plasma sheet to two interplanetary shocks: Tc-1 observations. *Chinese Science Bulletin*, *55*(6), 530–538. https://doi.org/10.1007/s11434-009-0345-6

Yu, Y., & Ridley, A. (2009). The response of the magnetosphere-ionosphere system to a sudden dynamic pressure enhancement under southward imf conditions. *Annales geophysicae*, *27*(12). 4391–4407. https://doi.org/10.5194/angeo-27-4391-2009

Zhang, X., Zong, Q.-G., Wang, Y., Zhang, H., Xie, L., Fu, S., et al.(2010). Ulf waves excited by negative/positive solar wind dynamic pressure impulses at geosynchronous orbit. *Journal of Geophysical Research*, *115*(A10). https://doi.org/10.1029/2009JA015016

Zuo, P., Feng, X., Xie, Y., Wang, Y., & Xu, X. (2015). Strong solar wind dynamic pressure pulses: Interplanetary sources and their impacts on geosynchronous magnetic fields. *The Astrophysical Journal*, *812*(2), 152–160. https://doi.org/10.1088/0004-637X/812/2/152